International Journal of Pharmaceutics 661 (2024) 124417

Contents lists available at ScienceDirect

International Journal of Pharmaceutics

journal homepage: www.elsevier.com/locate/ijpharm

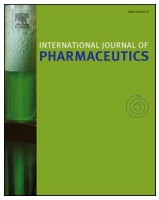

Supramolecular eutectogel as new oral paediatric delivery system to enhance benznidazole bioavailability

Beatrice Albertini [a,*], Serena Bertoni [a], Giorgia Nucci [a], Giada Botti [b], Michela Abrami [c], Stefano Sangiorgi [a], Sarah Beggiato [d], Cecilia Prata [a], Luca Ferraro [d], Mario Grassi [c], Nadia Passerini [a], Beatrice Perissutti [e], Alessandro Dalpiaz [b]

[a] Department of Pharmacy and Biotechnology, University of Bologna, Via San Donato 19/2, I-40127 Bologna, Italy
[b] Department of Chemical, Pharmaceutical and Agricultural Sciences, University of Ferrara, Via Fossato di Mortara 19, I-44121 Ferrara, Italy
[c] Department of Engineering and Architecture, University of Trieste, Via Alfonso Valerio, 6/1, I-34127 Trieste, Italy
[d] Department of Life Sciences and Biotechnology, University of Ferrara and LTTA Center, Via L. Borsari 46, I-44121 Ferrara, Italy
[e] Department of Chemical and Pharmaceutical Sciences, University of Trieste, Piazzale Europa 1, I-34127 Trieste, Italy

ARTICLE INFO

Keywords:
Natural deep eutectic solvents
Chagas disease
Rheology
Supersaturation
Pharmacokinetics
Oral delivery

ABSTRACT

Benznidazole (BNZ) serves as the primary drug for treating Chagas Disease and is listed in the WHO Model List of Essential Medicines for Children. Herein, a new child-friendly oral BNZ delivery platform is developed in the form of supramolecular eutectogels (EGs). EGs address BNZ's poor oral bioavailability and provide a flexible twice-daily dose in stick-pack format. This green and sustainable formulation strategy relies on the gelation of drug-loaded Natural Deep Eutectic Solvents (NaDES) with xanthan gum (XG) and water. Specifically, choline chloride-based NaDES form stable and biocompatible 5 mg/mL BNZ-loaded EGs. Rheological and Low-field NMR investigations indicate that EGs are viscoelastic materials comprised of two co-existing regions in the XG network generated by different crosslink distributions between the biopolymer, NaDES and water. Remarkably, the shear modulus and relaxation spectrum of EGs remain unaffected by temperature variations. Upon dilution with simulated gastrointestinal fluids, EGs results in BNZ supersaturation, serving as the primary driving force for its absorption. Interestingly, after oral administration of EGs to rats, drug bioavailability increases by 2.6-fold, with a similar increase detected in their cerebrospinal fluid. The noteworthy correlation between in vivo results and *in vitro* release profiles confirms the efficacy of EGs in enhancing both peripheral and central BNZ oral bioavailability.

1. Introduction

Benznidazole (BNZ) serves as the first-line treatment for patients with Chagas Disease (CD) and is included in the WHO Model List of Essential Medicines for Children (8th list, 2021). CD, also known as American Trypanosomiasis, is identified by the WHO as one of the primary Neglected Tropical Diseases (Campolmi et al., 2020). According to Pan American Health Organization, in Latin America at least one million women have CD, with the risk of transmitting the infection to their newborns, resulting in an estimated 8,000 to 15,000 infected babies born each year ("https://unitaid.org/news-blog/unitaid-commemorates-world-chagas-day-with-a-new-initiative-to-prevent-mother-to-child-transmission-of-the-disease/#en"). While most cases still occur in Latin America, the disease is increasingly spreading to other countries, including North America and Europe. CD is becoming a global issue with an estimated six to seven million people infected worldwide and 10,000 deaths attributed to the infection annually. After an acute phase characterised by high parasitemia, CD evolves into a chronic phase, corresponding to parasite penetration in the cardiac and digestive tissues, and brain. The acute phase induces inflammatory responses that can result in the death of 5–10 % of patients, primarily affecting children and immunosuppressed individuals (Echeverria and Morillo, 2019). Although the chronic phase is often asymptomatic, it can lead to irreversible damage to the oesophagus, colon, and heart, with heart-related complications being a leading cause of death (Urbina and Docampo, 2003). The BNZ treatment against CD appears very efficient in the acute phase (recovery up to 80 %), congenital cases (recovery higher than 95 %) and early chronic infections (recovery up to 70 %) (Urbina, 2010). In

* Corresponding author.
E-mail address: beatrice.albertini@unibo.it (B. Albertini).

https://doi.org/10.1016/j.ijpharm.2024.124417
Received 5 April 2024; Received in revised form 28 June 2024; Accepted 1 July 2024
Available online 2 July 2024

the acute phase, BNZ appears capable of protecting the cerebral microcirculation and reducing brain inflammation (Gonzaga et al., 2022). However, BNZ has several limitations, including its limited efficacy during the chronic phase, short terminal half-life, and low oral bioavailability, necessitating large drug doses and prolonged treatment durations, which increase the risk of adverse effects (Arrua et al., 2022; Arrúa et al., 2019). Specifically, in paediatric patients, the treatment regimen is 5 to 8 mg/kg/day orally administered in 2 divided doses, separated by about 12 h for a duration of 60 days (Pérez-Molina and Molina, 2018). Another significant problem is BNZ's poor aqueous solubility (0.23 mg/mL) and variable permeability, classifying the drug as either class II (de Moura Ferraz et al., 2018) or even class IV (Saatkamp et al., 2023) of the Biopharmaceutical Classification System (BCS). Irregular adsorption and erratic but always limited bioavailability were reported after BNZ oral administration (Arrúa et al., 2019). According to provisional paediatric BCS (pBCS), which is adapted to three paediatric subpopulations, namely neonates, infants and children, BNZ is classified as BCS class III and IV depending on the dose with a calculated log P of 1.64 (del Moral Sanchez et al., 2018). This classification suggests low solubility and permeability at high doses, indicating that more frequent administration of solubilized drug may improve absorption (del Moral Sanchez et al., 2018).

Over the past 12 years, various approaches have been undertaken to tackle BNZ variable bioavailability after oral administration (de Moura Ferraz et al., 2018) employing both bottom-up and top-down technologies. For instance, complexation with cyclodextrins (Leonardi et al., 2013; Soares-Sobrinho et al., 2012), solid dispersion approaches (Palmeiro-Roldán et al., 2014; Simonazzi et al., 2018), micronisation by solvent precipitation (Maximiano et al., 2011) and co-crystallization (Bezerra et al., 2020) have been studied to enhance BNZ solubility and/or dissolution rate. Moreover, solid formulations based on polyelectrolyte complexes or Eudragit RPO and L110-based microparticles have been investigated to reduce the frequency of administration and increase efficacy (Arrua et al., 2022; García et al., 2021). Furthermore, different lipid-based drug delivery systems, i.e., liposome drugs, SLNs and NLCs, have been designed to increase drug solubility and permeability (Scalise et al., 2016). Finally, liquid formulations, such as O/W nanoemulsions (Streck et al., 2019) and self-emulsifying delivery systems (Mazzeti et al., 2020) have been explored. However, these formulation strategies are accompanied by certain limitations regarding stability, reliance on organic solvents or extensive surfactant usage, and intricate manufacturing procedures. Not only do these challenges pose economic burdens, but they also diverge from the principles of "green chemistry" and sustainability. In this vein, Natural Deep Eutectic Solvents (NaDES), composed of bio-renewable ingredients and primary metabolites such as amino acids, sugars or organic alcohols, have recently emerged as a new type of solvent (Álvarez and Zhang, 2019; Dai et al., 2013; Liu et al., 2018). Often referred to as "the solvents of the 21st century", they are considered promising green vehicles capable of enhancing drug solubility (Albertini et al., 2023; Bazzo et al., 2020; Zainal-Abidin et al., 2019). These solvents are mixtures of two or more components that, at specific weight/molar ratios, form a viscous liquid system as a result of hydrogen interactions between a hydrogen bond donor (HBD) and acceptor (HBA). While applications of NaDES in the pharmaceutical field are still in their early stages, particularly for oral administration, previous studies have explored various mixtures. These studies have found that the mixtures constituted by proline: glutamic acid (1:1) and proline, malic acid, lactic acid and water (1:0.2:0.3:0.5) mostly increased the adsorption of low water-soluble phytochemicals such as rutin (Faggian et al., 2016) and berberine (Sut et al., 2017), respectively. Recently, NaDES composed of choline chloride and glycerol (1:3) were found to double the bioavailability of naringin, a poorly water-soluble flavonoid, in rats (Dangre et al., 2023).

To date, the cytotoxicity and pharmacokinetics of drugs integrated into eutectic systems have received limited investigation warranting further exploration. In this study, NaDES were initially investigated as potential solvents to improve BNZ solubility. Subsequently, they were utilised as intermediates in the development of xanthan gum-based eutectogels (EGs), which could be administered orally in a stick pack. This delivery method offers enhanced dose flexibility, ease of handling, and swallowing, particularly for children weighing $\leq$ 15 kg, compared to commercial paediatric tablets. NaDES-based EGs have recently emerged as a potential delivery platform for sunitinib malate (Mokhtarpour et al., 2020), quercetin (Xia et al., 2020) and curcumin (Bianchi et al., 2022). However, there is limited information available regarding the material properties and their in vivo behaviour. Here, BNZ-loaded EGs were investigated regarding rheological properties and *in vitro* release profiles using a paediatric gastrointestinal transit model. The cytotoxicity of BNZ-EGs on gingival fibroblast cell culture was assessed. Additionally, in vivo pharmacokinetic analysis was conducted in the bloodstream of rats following intravenous administration of BNZ and its oral administration as either solid raw drug or EGs formulations. Furthermore, to assess the capability of EGs in enhancing drug delivery to the CNS, the BNZ profile over time in the cerebrospinal fluid of rats of rats was assessed.

2. Materials and methods

2.1. Materials

Benznidazole (BNZ), N-benzyl-2-(2-nitroimidazol-1-yl) acetamide, was obtained from Sigma Aldrich (Milan, Italy). Choline chloride, Sodium Chloride (NaCl), L-(−)-malic acid, Glycerol, disodium hydrogen phosphate salt, potassium dihydrogen phosphate salt, L-glutamic acid monosodium salt hydrate) and DL-Tartaric acid were purchased from Sigma-Aldrich (Steinheim, Germany), while citric acid, D- (+)-glucose, L-proline, xylitol, sucrose, fructose and NaOH anhydrous pellets were obtained from Carlo Erba (Milan, Italy). Lactic acid 80 % (FG) and 90 % and Xanthan Gum (XG) were provided by Fagron (Bologna, Italy); while, hydroxypropylmethylcellulose (HPMC) (Methocel K200) was kindly donated by Colorcon (Dartford, UK). For Karl Fischer titration, Aquagent® Solvent and Aquagent® Titrant 5 (Scharlab, Barcelona, Spain) were used. Methyl-ferulate (Fer-Me), used as an internal standard for BNZ assay in the blood, was synthesised as previously described (Botti et al., 2022). Dimethyl sulfoxide (DMSO) and bovine serum albumin (BSA) were obtained from Sigma-Aldrich. Methanol, acetonitrile, ethyl acetate and water were of HPLC grade from Carlo Erba Reagents S.A.S. (Cedex, France). Dulbecco's phosphate buffered saline without calcium and magnesium (DPBS) was obtained by Thermo-Fisher Scientific (Milan, Italy). Male Sprague-Dawley rats were purchased from Charles River lab. (Calco, Italy).

2.2. Preparation and characterisation of unloaded NaDES

Overall, binary or ternary NaDES were prepared to start from solid raw materials, acting as HBA and HBD; when necessary, an accurate amount of water was added to allow ternary NaDES formation and/or to obtain a manageable consistency. In addition, liquid-based components (*e.g.*, lactic acid or glycerol) were used in some NaDES compositions, having the characteristics of good solvents for many organic compounds. Their composition is reported in Table 1.

Physical mixtures of the components in batches of 10 g were placed in screw-capped vials with stirring bars and heated within the temperature range of 50–85 °C. Finally, the mixture was allowed to cool down to room temperature (RT). The pH of NaDES was measured using a pH-meter (pH 80, XS Instruments, MO, Italy). The viscosity of eutectic mixtures was then assessed at RT using a viscometer (Visco Star-R, Fungilab S.A., Barcelona, Spain) with the spindle number TR8. The addition of small amounts of water corresponding to 2.5 and 5 wt% was also investigated.

Table 1
Composition, preparation conditions and pH of the examined NADES samples. N corresponds to NADES and RT indicates room temperature. *(ChCl = choline chloride, CA = citric acid, Fru = fructose, Gly = glycerol, Glu = glucose, LA = lactic acid, MA = malic acid, pro = proline, Su = sucrose, TA = tartaric acid, Xyl = xylitol)*.

NaDES	Samples	HBA: HBD: (water)	HBA:HBD: water weight *ratio*	water (%w/w)	T(°C)	pH
Choline chloride-based	N1	ChCl: Gly: H_2O	1:0.85:0.15	7.5	RT	5
	N2	ChCl: Glu:H_2O	5:2:0.7	10	80	4
	N3*	ChCl: Fru: H_2O	5:2:0.35	5	RT	5
	N4	ChCl: Xyl: H_2O	5:2:0.35	5	80	5–5.5
	N5*	ChCl:Suc	4:1	–	80–85	4
	N6	ChCl: Suc: H_2O	1:1:0.15	7.5	80–85	4
	N7	ChCl: Pro: H_2O	2:1:1.05	35	80	7
	N8	ChCl: CA: H_2O	3:1:0.4	10	80–85	2–2.5
	N9	ChCl: CA: H_2O	2:1:0.23	7.5	80	2–2.5
	N10	ChCl: LA	1:2	–	80	2
	N11	ChCl: TA: H_2O	2:1:0.23	7.5	80	1.5–2
	N12	ChCl: MA	1:1	–	85	1.5–2
Amino acid-based	N13	Pro: Glu: H_2O	1:1:0.8	40	80	6–6.5
	N14	Pro: Xyl: H_2O	1:1:0.8	40	80	7
	N15	LA: Glu	5:1	–	60	1.5–2
	N16	LA: Xyl	5:1	–	50	2–2.5
Organic acid-based	N17	CA: Glu: H_2O	1:1:0.35	17.5	80	1.5
	N18	CA: Glu: H_2O	1:1:1	35	60	1
	N19	LA:CA: H_2O	1:0.1:1	45	RT	1
	N20*	TA:Glu: H_2O	1:1:0.3	15	80	1.5–2

* Unstable NaDES which crystallised after one or more days.

2.3. HPLC analysis of BNZ

A reverse-phase HPLC method was developed to quantify BNZ in NaDES and EGs, for solubility experiments and *in vitro* drug release studies. Additionally, a separate HPLC method was developed and validated for pharmacokinetic analysis of BNZ in the bloodstream and cerebrospinal fluid of rats. Detailed descriptions of both HPLC methods are provided in the **Supplementary Data**.

2.4. Solubility studies

Solubility measurements of BNZ were conducted using the shake-flask method. An excess of BNZ was added to 10 mL of the selected medium and allowed to stir for a predetermined period of time. Tests were conducted in water at 25 °C for 24 and 48 h, while solubility measurements in Simulated Gastric Fluid (SGF, pH = 1.2) without pepsin and Simulated Intestinal Fluid (SIF, pH 6.8) without pancreatin (whose composition is reported in Scheme 1) were carried out at 37 °C for 48 h. For each sample, two supernatant aliquots of 1.5 mL were withdrawn, centrifuged at 10,000 rpm for 12 min, suitably diluted and quantified by HPLC. Solubility of BNZ in NaDES was performed at 25 °C after 24 and 48 h. Samples were centrifuged at 14,000 rpm (Eppendorf, Centrifugate 5810R) for 10 min. The supernatant was appropriately diluted with the mobile phase and analysed by HPLC. Furthermore, BNZ solubility was measured after the addition of 2.5 and 5 wt% of water to selected NaDES to evaluate the solubility trend with increasing water content. Finally, the solubility of BNZ was assessed in aqueous solutions containing different percentages of lactic acid (90 % and 80 %) for comparison with NaDES samples containing lactic acid as HBA. Three independent analyses were performed for each sample and the results were expressed as mean value ± SD. One-way analysis of variance (ANOVA) followed by the Bonferroni post hoc test (GraphPad Prism, version 7.0) was used to analyse the data; the level of significance was set at the probabilities of $*p < 0.05$, $**p < 0.01$ and $***p < 0.001$.

2.5. Preparation of BNZ-loaded eutectogels

The NaDES samples demonstrating the best solubility improvement were then prepared by loading a precise amount of BNZ to achieve about 5 or 10 mg/mL. The mixture was stirred for 24 h at 25 °C to enable the complete solubilization of BNZ. The final water content of the studied samples was calculated by Karl-Fischer titration (SI Analytics® Titro-Line® 7500 KF, Scharlab, Barcelona Spain). At least six runs were performed for each sample. Eutectogels (EG@N8, 9 and 12) were prepared

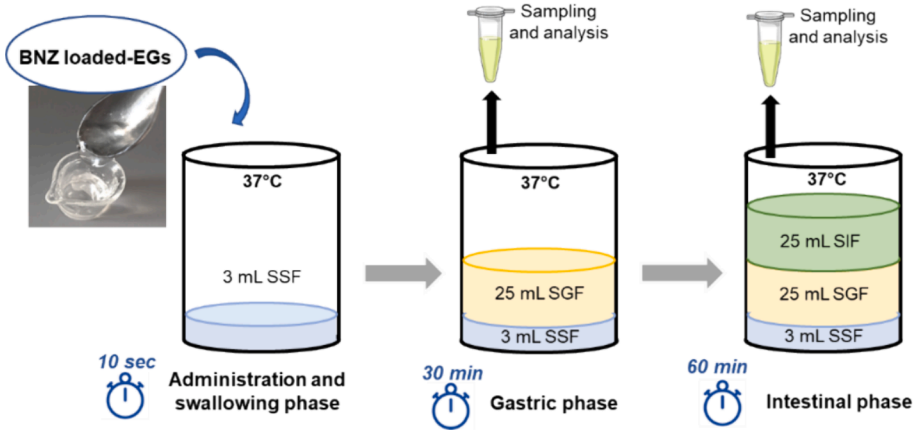

Scheme 1. Scheme of *in vitro* BNZ release experiments performed at 37 °C and stirring at 100 rpm. *Simulated Salivary Fluid* (SSF*): 2.38 g/L of Na_2HPO_4, 0.19 g/L KH_2PO_4, 8 g/L NaCl, the pH was adjusted to 6.8 using phosphoric acid [29]; *Simulated Gastric Fluid sine pepsin* (SGF^): 2.92 g NaCl/L, the pH was adjusted to 1.2 using a solution of HCl 37 %; *Modified-Simulated Intestinal Fluid sine pepsin* (SIF§): 6.8 g KH_2PO_4/0.5 L (0.1 M), the prepared basic solution was two-fold concentrated and the pH was adjusted to 11.14 to obtain a pH of 6.8 after mixing SGF with SIF.

Table 2
Composition, pH and BNZ concentration of gelled formulations. A theoretical BNZ loading amount of about 5 mg/mL and 10 mg/mL was considered for EG@N8-9–12 and EG@N15, respectively.

EGs	Gelling agent	water % (w/w)		pH	BNZ loading (mg/mL)
	Xanthan Gum (%, w/v)				
EG@N8	1	10		2.5–3	5.571 ± 0.122
EG@N9	1	10		2–2.5	5.477 ± 0.256
EG@N12	1	15		1.5–2	4.959 ± 0.027
	Gelling agent	**pH adjustment**		**pH**	**BNZ loading (mg/mL)**
	HPMC (% w/v)	**Na glutamate (mM)**	**NaOH 10 % (mL)**		
EG@N15	1	50	0.25	2–2.5	10.805 ± 0.105

by adding XG (1 % w/v) into the corresponding drug-loaded ChCl-based NaDES. These samples were stirred at RT and a suitable amount of water was added as reported in Table 2. Then, the mixtures were heated in a water bath at 80 °C for 15 min. EGs were allowed to cool down to room temperature and stirred for 72 h to enable the formation of limpid and homogeneous samples. For comparison, drug-free blank EGs were prepared using the same procedures. For LA-based NaDES (N15), a gelation process was obtained by adding HPMC at 1 % w/v, sodium glutamate (50 mM) and NaOH solution to adjust the pH value around 2.5–3. Their compositions and properties are reported in Table 2. The obtained samples were stored at RT and protected from light until used for characterisation and stability evaluation.

2.6. Characterization of drug-loaded eutectogels

2.6.1. Drug loading

Quantification of BNZ loaded into the gels was determined for each formulation prior to dissolution experiments. Aliquots of 25 μL for each sample were diluted with mobile phase at 1:400 *ratio* and BNZ amount was measured by the HPLC method. Three replicates were performed for each sample and the results were expressed as mean values ± SD. The BNZ content in EGs, packed in glass vials sealed with PE caps, was also assessed after storage at RT for 6 months

2.6.2. Fourier Transform-Infrared spectra (FT-IR)

Samples were mixed with anhydrous KBr, compressed using a hydraulic press (Perkin Elmer, Norwalk, CT, USA) and were analysed using a jasco FT-IR A-200 spectrophotometer (Pfungstadt, Germany) in the scanning range 400—4000 cm $^{-1}$ at the resolution of 1 cm^{-1}

2.6.3. Rheology

The rheological properties of BNZ-loaded EGs (Table 2) were studied by means of three typical rheological tests, i.e., the stress sweep, the frequency sweep and the steady value (flow curve) test. For comparison, a BNZ-loaded XG-based gel (XG gel) was prepared by dissolving the polymer (1 % w/V) in water at RT. Stress sweep, an oscillatory test working at a constant frequency (f = 1 Hz) and increasing stress amplitude, was used to detect the limit of the linear viscoelastic range over which the deformation causes sample micro-nano structure damaging. Frequency sweep tests, performed in the linear viscoelastic range (stress = 1 Pa), were led in the frequency range of 10–0.01 hz. The output of the frequency sweep tests, i.e., the dependence of the elastic (G') and viscous (G'') moduli on pulsation ω (=2πf), were determined as previously described (Lapasin and Pricl, 1995). A steady value (SV) or flow curve test was then performed to study the dependence of the sample shear viscosity (η) on the shear rate (γ). A detailed description of rheological methods is reported in Supplementary data. All rheological measurements were performed using a stress controlled rotational rheometer (Haake mars Rheometer, 379–0200 Thermo electron GmbH, Karlsruhe, Germany) equipped with a knurled plate-plate geometry (PP35, diameter = 35 mm). To prevent evaporation problems, sample characterization was conducted at 25 °C and 37 °C using a glass solvent trap

2.6.4. Low field NMR

The extinction of the x-y component (M_{XY}) of the magnetisation vector and the recovery of its z component (M_z) were measured at 37 °C employing a bruker minispec MQ20 (static magnetic field B_0 = 0.47 T, 20 MHz, Germany). Each sample was poured inside the glass tube (internal diameter 0.008 m) and sealed with a proper plastic top immediately after sample insertion. Then, the glass tube was maintained at 37 °C for ten minutes before measurement. Finally, it was rapidly inserted in the MQ20 sample holder positioned just above the magnetic field. The M_{XY} extinction (transversal relaxation) and m_z recovery (longitudinal relaxation) detection were performed as reported in the literature (Abrami et al., 2023) and are detailed in Supplementary data

2.7. In vitro drug release studies

Release tests were performed under non-sink conditions, more closely representing the oral administration of the BNZ slurry. Considering the treatment regimen of 5 mg/kg, a dose of 50 mg of BNZ is required for 10 kg infants. Due to the small gastric volumes, standard paddle experiments cannot be used; thus, a different setup of dissolution equipment was used: a total volume of 50 mL was considered applying a scaling factor of 2 of the drug's dose (Freerks et al., 2020). A detailed scheme of the test set-up is given in Scheme 1. Specifically, 25 mg of BNZ, as raw powder or gel samples (5 mL of EG@N8-9–12 or 2.5 mL of EG@N15, corresponding to 25 mg of BNZ) were first mixed with simulated salivary fluid (SSF) and then transferred into a flask containing 25 mL of SGF. Finally, 25 mL of the SIF was added into the flask. At predetermined time-points (after 1, 5, 10, 20, 30, 35, 45, 60, 75 and 90 min.), 500 μL samples were taken out, centrifuged and diluted 1:25 with the mobile phase and then filtered with nylon filters 0.2 μm into HPLC vials. The release profiles were compared by calculating the similarity factor (f_2). Two dissolution profiles are considered similar if the f_2 value is between 50 and 100.

2.8. MTT assay on Human gingival fibroblasts

MTT viability assay assessed the potential biocompatibility of unloaded and BNZ-loaded EGs in Human Gingival Fibroblasts (HGFs). HGFs were routinely cultured in Dulbecco's Modified Eagle Medium (DMEM) supplemented with 10 % foetal calf serum (FCS) at 37 °C and 5 % CO_2 and were not used beyond the fifth passage (Teti et al., 2015). HGFs were seeded at 2×10^4 cells/cm^2 and exposed to treatments after 1 day from the seeding. Cells (2×10^4/cm^2) were incubated with the different unloaded and loaded samples having theoretical BNZ concentrations of 5 mg/mL for EG@N8-9–12 or 10 mg/mL for EG@N15, respectively, for 24 h at 37 °C. The cells were then incubated with 5 mg/mL MTT solution for 4 h at 37 °C. Then, the MTT solution was removed and DMSO was added to dissolve the purple formazan salt crystals, formed during MTT reduction by cell metabolism (NADH). The absorbance was measured in a multiwell plate reader (Wallac Victor2, PerkinElmer) at 570 nm. Each experiment was performed three times, and four technical replicates were analysed in each experiment. The optical density obtained from treated cell cultures was expressed as the percentage of untreated cells (Control). Analysis of variance (ANOVA) followed by the Bonferroni post hoc test (GraphPad Prism, GraphPad software Inc., CA) was used to analyse the data (* $p < 0.05$).

2.9. In vivo administration of BNZ and pharmacokinetic studies

2.9.1. Intravenous administration of BNZ

Male Sprague-Dawley rats (about 250 g) were intravenously administered with 0.25 mg BNZ (1 mg/kg). In particular, a group of four rats, fasted for 24 h and anaesthetised during the experimental period, received a femoral IV administration of 0.25 mg/mL BNZ dissolved in a medium constituted by 20 % (v/v) DMSO and 80 % (v/v) physiological solution with a rate of 0.1 mL/min for 10 min. At the end of infusion and at fixed time-points blood samples (100 μL) were collected and cerebrospinal fluid (CSF) samples (about 30 μL) were withdrawn. For BZN quantification in blood and CSF samples, a novel procedure was developed (see Supplementary data for specific comments concerning literature). Practically, the blood samples were hemolysed with 500 μL of ice-cold water immediately after their collection, then 50 μL of 10 % sulfosalicylic acid and 50 μL of internal standard (100 μM Fer-Me dissolved in a water-methanol mixture 50:50 v/v) were added. The samples were extracted twice with 1 mL of ethyl acetate, and, after centrifugation at 13,000 x g for 10 min, the organic layer was reduced to dryness under a mild nitrogen stream at RT. Then, 150 μL of a water acetonitrile mixture (50:50 v/v) was added, and after centrifugation, 10 μL were analysed via HPLC for BNZ detection. As a control, each rat had a blood sample collected (100 μL) before the drug administration. The control samples were treated as above-described in the absence of the internal standard, substituted with the same volume of water-methanol mixture 50:50 (v/v). The CSF samples were withdrawn using the cisternal puncture method described by van den berg et al. (van den Berg et al., 2002), which requires a single needle stick and allows the collection of serial (about 30 μL) CSF samples that are virtually blood-free (Dalpiaz et al., 2008). A total volume of about a maximum of 120 μL of CSF/rat (i.e., four 30 μL samples/rat) was collected during the experimental session, choosing the time points (up to five, taking into account a maximum of four collections per rat) to allow the restoring of the CSF physiological volume. The CSF samples (10 μL) were immediately analysed via HPLC

2.9.2. Oral administration of BNZ and eutectogels

Male Sprague-Dawley rats (about 250 g) were orally fed with 2.5 mg BNZ (10 mg/kg), as solid free drug or as the EGs diluted in water. In particular, BNZ powder was mixed with palatable food to induce oral intake in a group of four rats. The other two groups (four rats/group), fasted for 24 h, received 1 mL of EG@N8 or EG@N12, diluted 1:1 in water immediately before their administration by gavage. The BNZ content in the diluted EGs was about 2.5 mg/mL. After the administration, blood (100 μL) and CSF samples (30 μL) were serially collected at fixed time points from each rat and treated as described above for the BNZ quantification. All in vivo experiments were performed under current italian legislation (D.L. 26/2014) that allows experimentation on laboratory animals only after approval by the ministry of Health (Rome, italy; authorisation n° 511/2022-PR), and in strict accordance with the european council directives on animal use in research (n. 2010/63/EU). Every effort was made to reduce the number of animals and their suffering

2.9.3. Pharmacokinetic calculations

The in vivo half-life ($t_{1/2}$) of BNZ in the bloodstream of rats was calculated by nonlinear regression (exponential decay) of concentration values obtained after intravenous infusion and confirmed by linear regression of the log concentration values versus time (semi-logarithmic plot). The area under the concentration–time curve (AUC, $\mu g \cdot mL^{-1} \cdot min$) related to intravenous and oral administration of BNZ in the bloodstream or CSF of rats was calculated by the trapezoidal method. The absolute bioavailability values (F) for the orally administered raw BNZ or BNZ formulated in the EGs were obtained as the ratio between the oral AUC and intravenous (IV) AUC values obtained for each compound and normalised with respect to their doses. The oral relative bioavailability values (RB) of the BNZ-loaded EGs formulations were calculated as the ratio between the oral AUC values of formulated and raw BNZ obtained in the bloodstream (more details are reported in **Supplementary Data**). All the calculations were performed by using graph pad Prism software, version 7 (GraphPad software Incorporated, LA Jolla, CA, USA)

3. Results

3.1. Evaluation of unloaded NaDES

Twenty combinations of HBA/HBD weight ratios were prepared and based on their composition, NADES were classified into three different groups, as shown in Table 1. The different weight ratios, the number of hydrogen bond donors and acceptors and the structure/position of bonds affected the stability of these solvents (Albertini et al., 2023; Dai et al., 2013). Specific comments are reported in **Supplementary data**.

Among the analysed combinations, only N3, N5 and N20 were unstable upon storage. Furthermore, except for N12 and samples containing LA, the addition of water to physical mixtures was necessary to reach the eutectic point. NaDES composed of organic acids showed low pH values, ranging from 1 to 2.5, while those with proline and sugars displayed higher pH values without exceeding neutrality. NaDES samples also differed in their viscosity, as shown in **Fig. S1**: N 6, 8, 9, 11, 12 and 17 showed higher viscosity values (range 1000–12,000 mP*s) in comparison to N 1, 2, 4, 10, 13, 15 and 16 (range 50–450 mP*s).

3.2. Benznidazole solubility in NADES

The solubility of BNZ in water was 201.95 ± 18.41 μg/mL after 24 h at RT and it slightly increased after 48 h at 204.50 ± 21.53 μg/mL in agreement with previously reported data (Santos Souza et al., 2017). The results of BNZ solubility in NaDES after 24 and 48 h are reported in Fig. 1**A**. Remarkably, most eutectics significantly enhanced BNZ solubility compared to water after 24 h, regardless of their pH. The highest solubility values were achieved with ChCl-based mixtures (N1-N12) and those containing LA (N10, N15 and N16). Specifically, among the ChCl-based NaDES, those with choline/organic acids such as citric acid and malic acid (N8, N9 and N12) exhibited the most substantial increment, as evidenced in Table 3.

The lowest solubility was observed with N14 and N13 (neutral pH, Table 1) and N18 (very acidic) with concentrations ranging between 800–1100 μg/mL. Proline-based NaDES and mixtures containing sugars/organic acids with a high percentage of water (40 % w/w added to the HBA:HBD mixture, as shown in Table 1) were not as effective as choline chloride-based ones in enhancing BNZ solubility. After 48 h (Fig. 1**A**), most analysed NaDES did not exhibit significant changes in solubilized BNZ. However, sample N17 showed a significant solubility enhancement after 48 h ($p < 0.001$).

Data suggest that the solubilising capacity of NaDES is primarily influenced by water content: N8 and 9 have a lower water amount (10 %-7.5 % w/w, respectively), while N12, having the most significant solubility enhancement (36-fold), did not contain water. Accordingly, further addition of water to these samples (Fig. 1**B**), besides the lowering in viscosity (Fig. S1A), decreased drug solubilisation to various extents. In particular, the addition of water in N9 had a lower impact on BNZ solubility compared to N8 and N12. The addition of 2.5 % water to N8 or N12 led to a significant variation in BNZ solubility ($p < 0.001$) whereas a further addition of 2.5 % water caused an additional drop in drug solubility only for N12. In contrast, N9 was the sample least affected by water dilution ($p > 0.05$).

Among all the analysed NaDES, BNZ solubility increased by nearly 100-fold in the case of N10, N15 and N16, as shown in Fig. 1**A**. All these mixtures included lactic acid (90 %) either as HBA (N10) or HBD (N15 and N16); indicating that lactic acid is a good solvent for BNZ. After 48 h, the drug solubility increased only for N15. Following dilution with 2.5

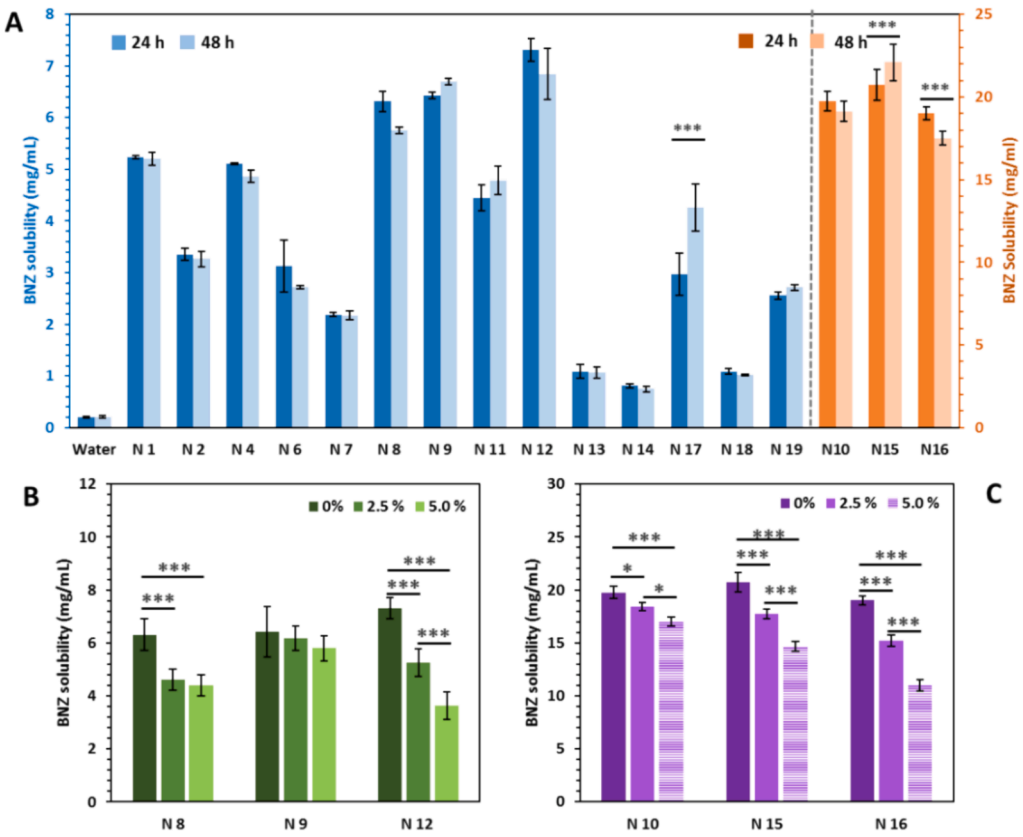

Fig. 1. A) Solubility values of BNZ in stable NaDES at 24 ad 48 h; N10, N15 and N16 refer to the right scale; Effect of water addition (0, 2.5 and 5 %) on the solubility of BNZ **B)** in NaDES obtained starting from solid components and with the best solubility enhancement **C)** in NaDES containing lactic acid. (Bars indicate SD (n = 3); * $p < 0.05$, ** $p < 0.01$ and *** $p < 0.001$).

Table 3
Solubility values of BNZ in water and in NaDES with 0, 2.5 and 5% w/w extra-water.

Samples	BNZ solubility (μg/mL) ± SD (24 h and 25 °C)			Solubility increment
	0 % water	*2.5 % water*	*5 % water*	
Water 25 °C	201.95 ± 18.41	–	–	
N8	6315.76 ± 192.92	6276.54 ± 126.59	4396.39 ± 206.31	30
N9	6431.69 ± 57.88	6183.08 ± 116.72	5797.78 ± 225.29	31
N12	7309.10 ± 224.70	5254.37 ± 283.49	3642.65 ± 147.4	36
N15	20736.75 ± 947.98	17737.03 ± 466.11	14700.00 ± 515.35	103

and 5 wt% of water, BNZ solubility decreased significantly (Fig. 1**C**) though it still reached high values (>11 mg/mL). Determination of BNZ solubility in lactic acid solutions at different concentrations (90 % vs 80 %) was then carried out and compared with the solubility values of N15 (**Fig. S2**). The results confirmed that lactic acid at 90 % is an excellent solvent for BNZ; but its solubility substantially dropped when the LA amount decreased, as in the case of LA at 80 % and N15.

3.3. Preparation and characterisation of eutectogels

Using the solubility results as a guide, four NADES-based eutectogels (EG@N) were prepared (Table 2). Initially, the actual amount of water in the selected ChCl-based NaDES (N8, N9, and N12) was analysed by Karl Fischer titration. The results indicated that the measured water contents closely matched the theoretically added water, specifically 12.6 ± 4.4 %, 8.22 ± 3.6 %, and 0.7 ± 0.6 % for N8, N9, and N12, respectively. With these samples, clear EGs formed using xanthan gum at 1 % w/v along with an appropriate amount of water (as specified in Table 2). This was followed by an annealing treatment at 80 °C for 15 min. In contrast, EG@N15 was formed by replacing XG with HPMC at a concentration of 1 % w/w. Then, a buffer system was then added to adjust its pH around 2–2.5. The BNZ concentration in each sample is reported in Table 2 demonstrating that the drug loading was very close to the theoretical one.

The appearance of EGs upon storage at RT remained unchanged without evidence of drug crystals or phase separation. The results of drug loading, reported in **Table S1** confirmed that BNZ content did not change significantly ($p > 0.05$).

3.3.1. In vitro drug release profiles from eutectogels

Release experiments under non-sink conditions were performed to evaluate if NaDES included in the gel formulations may affect the release profiles of BNZ. In order to do so, firstly BNZ solubility was analysed in both SGF and SIF at 37 °C for 48 h: the results were 256.15 ± 3.20 μg/mL and 205.65 ± 1.38 μg/mL, respectively, close to the values obtained in water at 25 °C. These results are consistent with the BNZ pH independent-solubility, as already shown by Maximiano et al., which found similar log P values using different aqueous media (Maximiano et al., 2010).

Fig. 2**A** shows the mean concentration–time profiles over a time interval of 90 min in SSF and the gastro-intestinal simulated fluids (SGF and SIF). After the dilution of EGs with the small volume of SSF, BNZ remained molecularly dispersed within the supramolecular structure. Considering the first 30 min in the SGF, all samples reached a faster and higher drug concentration when compared to the raw powder ($f_2 < 50$, **Table S2**), establishing a supersaturated condition. The drug

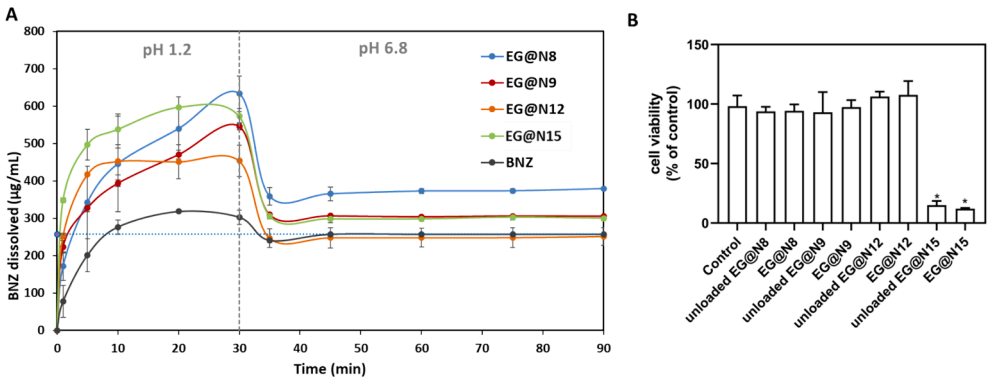

Fig. 2. A) Release profiles of eutectogels in comparison to raw BNZ (black line); bars indicate SD (n = 3). The dashed grey line indicates the BNZ equilibrium solubility in SGF at 37 °C. **B)** Cell viability of HGFs exposed to different unloaded and loaded oral formulations for 24 h. Values are expressed as mean (n = 3) ± SD of the relative percentage compared to control HGFs (Control). *Represents a significant difference compared to HGFs control, *P < 0.05.

concentration reached its maximum within 30 min, decreasing after that due to dilution with SIF, until it reached constant values. Among the different EG@N, a significant improvement in BNZ concentration was observed in EG@N8, demonstrating an oversaturated sustained condition in both gastric and intestinal tracts (Table S2). Its drug release profile in SGF was quite similar to that of EG@N9 ($f_2 = 55.5$), being both composed of ChCl and CA. In contrast, the EG@N12 release profile showed the achievement of a concentration plateau within 30 min, which decreased to the values of raw BNZ after the pH shift. EG@N15 displayed a more rapid increase in drug release within the first 10 min than EG@N8 ($f_2 = 49.1$), but the final drug concentration remained significantly lower ($f_2 = 41.8$).

3.3.2. *Evaluation of potential cytotoxicity of the formulations*

To evaluate the potential cytotoxicity of the different formulations, the MTT assay was performed using HGFs treated with unloaded and loaded EG@N for 24 h. As shown in Fig. 2**B**, none of the tested formulations reduced cell viability except for the LA-containing formulation (EG@N15). The loading of EG@N with BNZ generally didn't affect cell viability under the tested experimental conditions. Considering these results, LA-based eutectics were discarded, and only EGs formulations prepared using N8, N9 and N12 were further characterised and used for pharmacokinetic (PK) studies.

3.3.3. *FT-IR assay*

The FT-IR analysis was performed on BNZ loaded and unloaded EG@N samples and the spectra (shown in Fig. S3) were compared to neat NaDES to evaluate possible specific interactions among components after the gelation. Results, discussed in detail in Supplementary data and summarised in Table S3, indicate that the NaDES structure remained substantially unaltered in the final drug-loaded EG@N. The gel formation and BNZ loading mainly affected the C-N stretching of ChCl and the H-bonding network between water, polymer and NaDES components, especially for EG@N8, supporting the extensive interactions within the supramolecular assembly.

3.3.4. *Rheological behaviour of eutectogels*

Fig. 3**A** shows the output of the frequency sweep test (the so-called

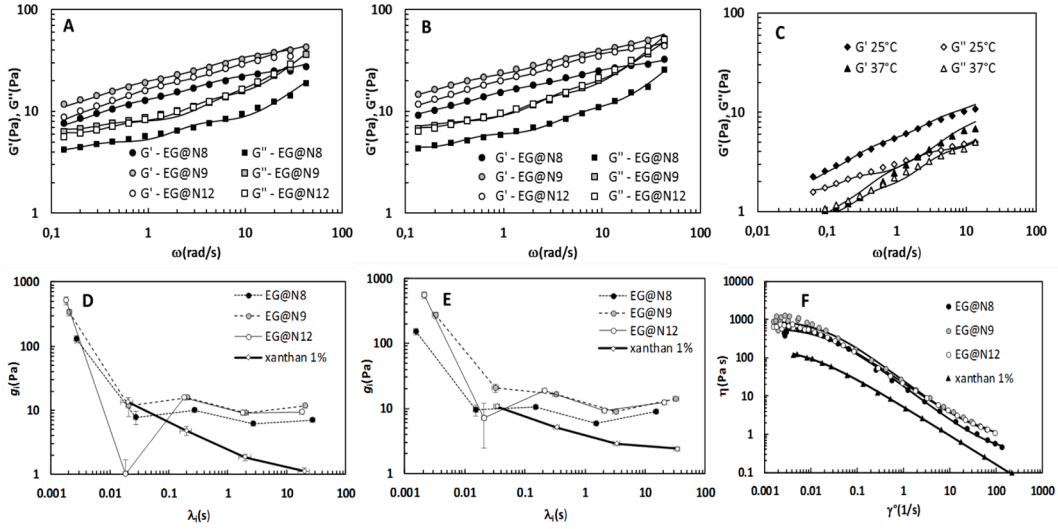

Fig. 3. A) Frequency sweep tests of EGs performed at 37 °C and **B)** at 25 °C. Circles represent the elastic modulus G', while squares indicate the viscous modulus G''. Solid lines indicate eq.(**S1**) and eq.(**S2**) best fitting. The statistic F_{test} reads: **A)** $F_{EG@N8}$ (5, 28, 0.95) < 757; $F_{EG@N9}$ (6, 26, 0.95) < 1073; $F_{EG@N12}$ (5, 24, 0.95) < 1331**B)** $F_{EG@N8}$ (5, 26, 0.95) < 906; $F_{EG@N9}$ (5, 26, 0.95) < 1083; $F_{EG@N12}$ (4, 25, 0.95) < 357. **C)** Frequency sweep tests performed at 37 °C and 25 °C regarding the XG gel. Filled symbols indicate the elastic modulus G', and open symbols represent the viscous modulus G''. Solid lines are eq.(**S1**) and eq.(**S2**) best fitting. The statistic F_{test} reads F_{37} (4, 25, 0.95) < 126; F_{25} (5, 26, 0.95) < 922. **D)** Relaxation spectra referring to EGs and XG gel at 37 °C and **E)** *at* 25 °C. Vertical and horizontal bars indicate the standard deviations referring to eq.(**S1**) – (**S2**) fitting parameters (λ_i, g_i). Lines are simply guides for the eye. ***F***) Steady value test (flow curve) (37 °C) referring to the EGs plus the XG gel. η and (γ) are, respectively, shear viscosity and shear rate. Solid lines indicate eq.(**S4**) best fitting. The statistic F_{test} reads $F_{EG@N8}$ (3, 23, 0.95) < 240; $F_{EG@N9}$ (3, 25, 0.95) < 140; $F_{EG@N12}$ (3, 26, 0.95) < 1059; $F_{xanthan}$ (3, 12, 0.95) < 1288.

mechanical spectrum) referring to the three considered EG@N. These samples can be considered weak gels as the elastic modulus *G*' was always bigger than the viscous one *G*'' (*G*' ≈ 2–3 times *G*'') in the pulsation (ω) range considered. In addition, *G*' and *G*'' trends vs ω were parallel and not too dependent on ω. Three mechanical spectra could be noticed to be similar even if EG@N9 is the strongest one (highest *G*' and *G*'') while EG@N8 was the weakest one (lowest *G*' and *G*''). Fig. 3**B** clearly demonstrates that the temperature reduction from 37 °C to 25 °C did not imply important variations in the mechanical spectra of the three EG@N samples. On the contrary, Fig. 3**C** shows that, at 37 °C, the XG gel represents the typical sol–gel transition condition as *G*' and *G*'' were almost coincident in the whole ω range considered. Conversely, at 25 °C (Fig. 3**C**), the mechanical spectrum of XG gel undergoes a considerable variation characterised by a prevalent increase of *G*' compared to *G*'' (*G*' > *G*'', *G*' and *G*'' parallelism) indicating weak gel behaviour. From these experimental data (whose reliability is proven by the statistic F_{test} – see captions to Fig. 3**A, B, and C**) the relaxation spectrum (a sort of sample rheological identity card – Fig. 3**D and E**) and the shear modulus (stiffness, *G* – Table 4) of each sample were obtained. Fig. 3**D-E** and Table 4 evidenced that temperature variation did not significantly alter either the G values or the relaxation spectrum of EG@N. On the contrary, temperature variation modified the XG gel relaxation spectrum which changed from the typical liquid solution shape (g_i decrease with λ_i) at 37 °C to that of a gel (small or negligible g_i variation with λ_i) at 25 °C, while not altering the shear modulus G.

Interestingly, relaxation spectra values for EG@N are very similar to each other and suggested the presence of two structures: a prevailing faster relaxing structure (λ_1, g_1) coexisting with a slower relaxing structure identified by the other four spectrum elements (λ_2, g_2; λ_3, g_3, λ_4, g_4; λ_5, g_5). These g_i values (g_2-g_5), which were similar to each other, were much smaller than g_1, resembling a typical slow relaxation spectrum of hydrogels. The obtained values indicated that the former structure is abundant (high g1) and characterised by labile crosslinks due to weak interactions (small λ_1), while the latter showed much more intense and stable crosslinks (higher λ_i), albeit much less abundant as indicated by $(g_2 + g_3 + g_4 + g_5) \ll g1$.

The steady value test (flow curve), shown in Fig. 3**F**, demonstrates clear non-Newtonian behaviour of EG@N and of XG gel as their shear viscosity (η) is almost constant for low shear rates (γ) to subsequently decrease for higher shear rates (the typical rheological behaviour of polymer melts and polymer solutions). This behaviour implies the existence of a labile internal structure undergoing a significant variation induced by a high shear rate. All the EG@N show similar rheological behaviour (Fig. 3**F**), even if, as in the case of the frequency sweep test, EG@N9 is the most viscous sample and EG@N8 the least viscous (see also the eq.(**S4**) fitting parameters reported in **Table S4**). EG@N12 showed the greatest contribution to the elastic component (highest G, Table 4); however, under flow conditions (Fig. 3**F**), the viscous characteristics prevailed over the elastic ones and EG@N9 offered the greatest flow resistance. Finally, XG gel exhibits a shear viscosity which is much lower than that of EG@N, as shown in **Table S4**.

The rheological characterisation of the original solutions (N8, N9, N12) was undertaken as well. Frequency sweep test revealed that their rheological behaviour is that of a liquid system as the elastic modulus (*G*') is always negligible (about two orders of magnitude lower) to the viscous one (*G*'') (data not shown). In addition, the flow curve (**Fig. S4**) test conclusion demonstrates that all of them (N8, N9, N12) are Newtonian fluids as their viscosity does not change with shear rate despite being characterised by different viscosities at 37 °C (η_{N8}(Pa*s) = (0.100 ± 0.003); η_{N9}(Pa*s) = (0.650 ± 0.034); η_{N12}(Pa*s) = (4.50 ± 0.44)).

Table 4
Shear modulus (*G*) competes with the EGs and the XG gel at 37 °C and 25 °C.

	G(Pa) 37 °C	***G***(Pa) 25 °C
EG@N8	159 ± 16	187 ± 41
EG@N9	388 ± 39	332 ± 29
EG@N12	548 ± 70	600 ± 60
XG gel	21 ± 2	21 ± 1

3.3.5. Low-field NMR measurements

Eq.(**S5**) and eq.(**S6**) were fit to experimental data as shown in Fig. 4**A-B**, where the magnetic relaxation of EG@N9, N9, and XG gel are shown as representative examples, as the magnetic relaxation properties of all EGs were similar. Indeed, not only did they have similar average longitudinal (T_{1m}) and transversal (T_{2m}) relaxation times, but their components also showed similar relaxation times (T_{1i} or T_{2i}) and % weight ($A_{i\%}$) (**Table S5**). On the contrary, a notable difference in relaxation times (both longitudinal and transversal) was detected between EG@N and NaDES as well as between EG@N and XG gel. Indeed, the average relaxation times (T_{1m}, T_{2m}) of XG gel were one order of magnitude higher than those of EG@N, while T_{1m} and T_{2m} of NaDES were about 1/2—1/3 to those of EGs. Thus, as seen in the case of the rheological characterisation, NaDES jellified by XG (plus 10 % − 15 % water) provides systems with very different magnetic relaxation properties. Finally, it is worth noticing that both T_{1m} and T_{2m} decrease moving from N8, N9 to N12, this being reasonably due to the reduction of water content. It is well known that water transversal relaxation time (longitudinal relaxation time is bigger) is around 4 s at 37 °C applying a static magnetic field B_0 = 0.47 T (Coviello et al., 2013). Eq.(**S9**) − eq.(**S10**) fitting to relaxation data (Fig. 4**A-B**) allowed us to get the continuous magnetic relaxation spectrum whose shape is depicted in Fig. 4**C** for the representative case of EG@N9. Following the discrete relaxation spectrum (Table S5), the continuous spectrum reveals two peaks that closely align with the discrete distribution. The statistics F_{test} proved the reliability of eq.(**S9**) and (**S10**) fitting to experimental data, as shown by the values of the fitting parameters reported in **Table S6**.

The strategy adopted to fit the relaxation data (i.e., eq.(**S9**) and (**S10**)) allowed us to determine the T_1 and T_2 distribution separately and to obtain the T_1-T_2 surface. Indeed, provided that T_1 and T_2 distributions are similar (Song et al., 2002)(we found a very significant correlation (r_{sp} = 0.192, $p < 0.0064$) among the continuous T_1 and T_2 distribution intensities), the 2D surface can be represented by the product of eq.(**S9**) and eq.(**S10**) evaluated at different points on the T_1-T_2 surface, as depicted in Fig. 4**D**. The plot clearly shows the existence of two peaks, the most important of which centred around $T_2 \approx 190$ ms and $T_1 \approx 190$ ms.

3.4. Pharmacokinetics

3.4.1. Intravenous administration of BNZ

BNZ was administered to rats at a dose of 250 μg (1 mg/kg) via intravenous infusion completed within 10 min. At the end of infusion, a plasmatic concentration of 10.1 ± 0.4 μg/mL was detected. This concentration decreased over time (Fig. 5**A**) following apparent first-order kinetics, as confirmed by the linearity of the semilogarithmic plot reported in the inset of Fig. 5**A** (n = 7, r = 0.997, P < 0.0001). The BNZ half-life was 105.5 ± 3.4 min. The AUC value in the bloodstream obtained by the 250 μg BNZ infusion from its starting time to infinity was 1461 ± 29 $\mu g \cdot mL^{-1} \cdot min$ (Table 5).

After the intravenous administration of BNZ, its concentration in the CSF of rats (Fig. 5**B**) increased up to 3.63 ± 0.15 μg/mL (C_{max}) within 30 min (T_{max}), then decreased to 0.43 ± 0.02 μg/mL within 180 min from the end of infusion. The AUC value of the BNZ profile in CSF, from the start of infusion to 180 min, was 313.4 ± 8.8 $\mu g \cdot mL^{-1} \cdot min$ (Table 5). The concentration ratio values of BNZ between CSF and bloodstream at 30 and 60 min from the end of infusion were 0.46 ± 0.03 and 0.47 ± 0.04, respectively. These values, very near to 0.5, indicate a marked aptitude of BNZ to permeate in the central nervous system from the bloodstream, suggesting the ability of this drug to counteract the Chagas disease at both peripheral and central levels.

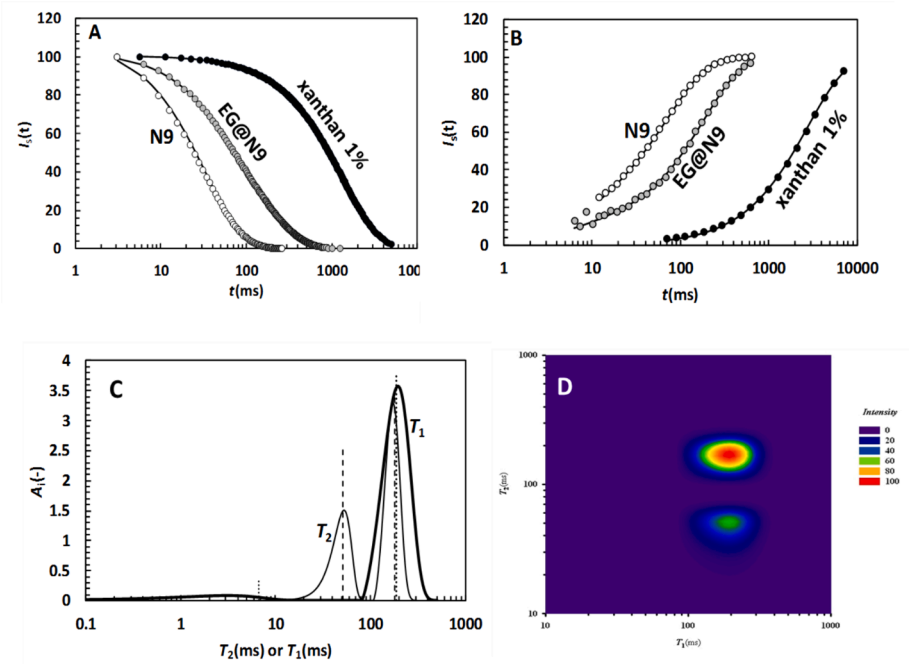

Fig. 4. **A**) Magnetic relaxation intensity (I_s) referring to N9, EG@N9 and XG gel (transversal relaxation (T_2)) (solid line indicates eq.(**S5**) best fitting). F_{test} reads: $F_{EG@N9}(3, 189, 0.95) < 3*10^6$; $F_{N9}(3, 82, 0.95) < 8.6*10^4$; $F_{xanthan}(1, 201, 0.95) < 2*10^8$. **B**) Magnetic relaxation intensity (I_s) referring to N9, EG@N9 and XG gel (longitudinal relaxation (T_1)) (solid lines indicate eq.(S6) best fitting). F_{test} reads: $F_{EG@N9}(3, 26, 0.95) < 3*10^4$; $F_{N9}(3, 26, 0.95) < 1.1*10^5$; $F_{xanthan}(1, 18, 0.95) < 2.3*10^4$. **C**) Continuous magnetic relaxation spectrum of sample EG@N9. While the thin line refers to the transversal (T_2) spectrum, the thick line refers to the longitudinal (T_1) spectrum. Dotted vertical lines indicate the position of the "discrete" distribution reported in **Table S5**. Their lengths are proportional to the intensity $A_{1\%}$ and $A_{2\%}$ competing to the couples T_{21}-T_{22} or T_{11}-T_{12} reported in **Table S5**. **D**) Two-dimensional T_1- T_2 surface referring to EG@N9. For clarity of presentation, intensities have been normalised to the maximum value of the eq.(**S9**) and eq.(**S10**) products.

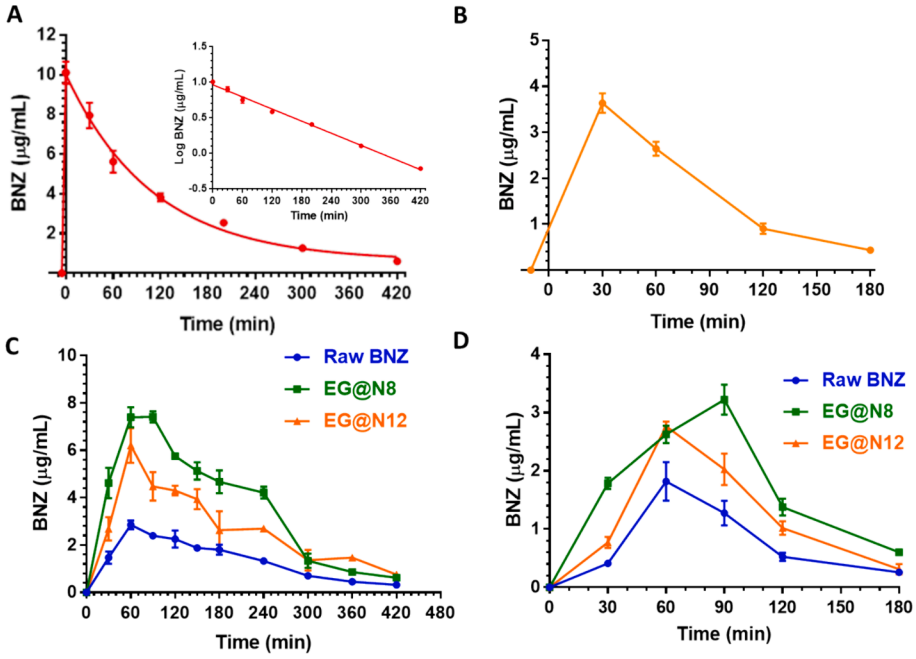

Fig. 5. **A**) Elimination profile of BNZ after 0.25 mg (1 mg/kg) infusion to rats. The elimination followed an apparent first-order kinetic, confirmed by the semi-logarithmic plot reported in the inset (n = 7, r = 0.997, P < 0.0001). The half-life of BNZ was calculated to be 105.5 ± 3.4 min. All data are expressed as the mean ± S.E. of four independent experiments. **B**) BNZ concentrations (μg/mL) detected in the CSF of rats after the intravenous infusion of 0.25 mg (1 mg/kg). The data are expressed as the mean ± S.E. of four independent experiments. **C**) Blood BNZ concentrations (μg/mL) within 420 min following oral administration of 10 mg/kg doses to rats. Data are expressed as the mean ± S.E. of four independent experiments. The oral formulations consisted of raw BNZ mixed with palatable food (Raw BNZ), or formulated as EG@N8 or EG@N12 diluted 1:1 in water. **D**) Cerebrospinal fluid BNZ concentrations (μg/mL) within 180 min following oral administration of 10 mg/kg doses to rats. Data are expressed as the mean ± S.E. of four independent experiments. The oral formulations consisted of raw BNZ mixed with palatable food (Raw BNZ), or formulated as EG@N8 or EG@N12 diluted 1:1 in water.

Table 5
Area under Curve (AUC), absolute bioavailability and relative bioavailability values obtained in the bloodstream of rats and area under Curve (AUC) values obtained in the CSF of rats after the intravenous or oral administration of BNZ. The data are reported as the mean ± S.E. of four independent experiments.

Formulation	Administration form	Dose (mg/Kg)	Bloodstream			CSF
			AUC ($\mu g \bullet mL^{-1}$ min)	Absolute bioavailability	Relative bioavailability[a]	AUC ($\mu g \bullet mL^{-1}$ min)
Free BNZ	Iv infusion	1	1461 ± 29	–	–	313.4 ± 8.8
Raw BNZ	Oral[b]	10	615 ± 13	4.2 ± 0.2 %	–	136.6 ± 8.7
EG@N8[c]	Oral (by gavage)	10	1619 ± 30	11.1 ± 0.4 %	263 ± 9 %	309.0 ± 8.3
EG@N12[c]	Oral (by gavage)	10	1237 ± 41	8.5 ± 0.5 %	201 ± 9 %	222.1 ± 7.9

[a] concerning raw BNZ.
[b] mixed with palatable food.
[c] diluted in water (1:1 v/v).

3.4.2. Oral administration of BNZ

The dose chosen for the oral administration of raw BNZ was related to the drug content in the formulations EG@N8 and EG@N12 (Table 3) and after their dilution 1:1 in water was about 2.5 mg/mL. Dilution of EG@N formulations was required to manage them during oral administration to rats by gavage. The volume of orally administered EGs was 1 mL, therefore the BNZ oral dose was about 2.5 mg (10 mg/kg). For the oral administration of raw BNZ to rats, 2.5 mg of the drug was mixed with palatable food, resulting in the highest concentration in the bloodstream at 60 min (T_{max}) with a value of 2.85 ± 0.13 μg/mL (C_{max}), which decreased to 0.323 ± 0.004 μg/mL at 420 min, as reported in Fig. 5**C**. The AUC value of the BNZ profile, here calculated from the time 0 to infinity, was 615 ± 13 $\mu g \cdot mL^{-1} \cdot min$ which allowed the calculation of the absolute bioavailability (F) value of 4.2 ± 0.2 % (Table 5). This result indicates a relatively poor aptitude of BNZ to be absorbed in the bloodstream of rats after its oral administration in the raw form. Despite the relatively low raw BNZ oral F value, the presence of this drug was quantifiable in the CSF of rats after the oral administration of 10 mg/kg in the raw form. Indeed, as reported in Fig. 5**D**, the C_{max} value of BNZ in CSF was 1.82 ± 0.23 μg/mL at 60 min (T_{max}), which decreased to 0.26 ± 0.04 μg/mL at 180 min; the CSF concentration profile allowed for the calculation of an AUC value, between 0 and 180 min, of 136.6 ± 8.7 $\mu g \cdot mL^{-1} \cdot min$ (Table 5). This area value, normalised relative to the intravenous infusion dose, indicates a BNZ transit in the CSF of rats after oral administration, corresponding to the 4.4 % of that obtained after its intravenous administration. This aspect confirms the poor oral bioavailability of BNZ. However, it also indicates that the high permeation to the central nervous system from the bloodstream is maintained after oral administration. The concentration ratio values of BNZ between CSF and bloodstream at 30, 60 and 90 min from the end of infusion were 0.28 ± 0.04, 0.64 ± 0.11 and 0.51 ± 0.07, respectively. The mean ratio (0.48 ± 0.11) appears similar to that obtained between 30 and 60 min after intravenous drug administration (0.47 ± 0.01). These data suggest that the potential ability of BNZ to counteract Chagas Disease at the central level (indicated by the drug presence in the CSF of rats after the intravenous infusion, Fig. 5**B**), should not be altered after the oral administration of the drug if appropriate doses are used.

The oral administration to rats of EG@N8 and EG@N12 at the same dose of the raw drug (10 mg/kg) induced a significant bioavailability increase of BNZ, as evidenced in Fig. 5**C**. In particular, EG@N8 and EG@N12 allowed to obtain C_{max} values in the bloodstream at 60 min (T_{max}) of 7.39 ± 0.30 μg/mL and 6.20 ± 0.52, which decreased at 420 min to 0.63 ± 0.05 μg/mL and 0.76 ± 0.02 μg/mL, respectively. The AUC values of the BNZ profiles, calculated from time 0 to infinity, were 1619 ± 30 $\mu g \cdot mL^{-1} \cdot min$ for EG@N8 and 1237 ± 41 $\mu g \cdot mL^{-1} \cdot min$ for EG@N12, corresponding to absolute bioavailability (F) values of 11.1 ± 0.4 % and 8.5 ± 0.5 %, respectively (Table 5). The relative bioavailability values (obtained by comparison with the oral administration of the raw drug, Table 5) of EG@N8 (263 ± 9 %) and EG@N12 (201 ± 9 %) indicate that these formulations allow for an increase of up to 2.6 times in the oral absorption of BNZ in the bloodstream, in comparison to the raw drug. A similar behaviour was observed in the CSF, after the oral administration of the EG@N. In particular, as reported in Fig. 5**D**, the CSF BNZ C_{max} values were obtained at 90 and 60 min with values of 3.22 ± 0.18 μg/mL and 2.76 ± 0.06 μg/mL for EG@N8 and EG@N12, respectively. These values decreased to 0.60 ± 0.04 μg/mL and 0.31 ± 0.06 μg/mL at 180 min; the overall CSF concentration profile allowed for the calculation of AUC values, between 0 and 180 min, of 309.0 ± 8.3 $\mu g \cdot mL^{-1} \cdot min$ and 222.1 ± 7.9 $\mu g \cdot mL^{-1} \cdot min$ for EG@N8 and EG@N12, respectively (Table 5), indicating their ability to increase the BNZ absorption in the central nervous system up to 2.3 times, in comparison to the oral administration of a same dose of the raw drug.

4. Discussion

Recently, a child-adapted dose of 12.5 mg of BNZ per tablet has been formulated for children of 2 to 12 years to improve dosing accuracy, safety and adherence to therapy. For children weighing less than 15 kg, the recommended dose is 50 mg, thus corresponding to 4 tablets. Preschool-aged children, who are unable to swallow tablets, are generally treated with 12.5 mg tablet slurry by crushing or directly dispersing the tablet in water or orange juice according to the scheme reported in the FDA prescribing information ("https://www.accessdata.fda.gov/drugsatfda_docs/label/2017/209570lbl.pdf"). A recent study reported the pharmacokinetic of BNZ paediatric tablets in infected children ranging from new-borns to 12-year-olds. The study showed that the treatment was effective and well-tolerated, although children had lower blood levels of BNZ compared to adults receiving similar weight-adjusted doses (7.5 mg/kg/day) for 60 days (Altcheh et al., 2023). However, tablet manipulation can lead to dosing errors, along with issues such as poor palatability and the risk of administering toxic or sub-therapeutic doses. Therefore, it is of great interest to improve BNZ solubility and its overall bioavailability in order to reduce its dosage, but also to develop new age-appropriate paediatric formulations that are safe, compliant, and easy to administer (del Moral Sanchez et al., 2018).

To address these challenges in the treatment of CD, NaDES are proposed as new solvents for boosting the solubility of poorly water-soluble BNZ, due to their simplicity of preparation, sustainability and low cost (Álvarez and Zhang, 2019). The solubility results confirm the effectiveness of NaDES in enhancing the BNZ solubilisation (Fig. 1**A**); particularly the supramolecular assembly formed by choline chloride with either citric acid or malic acid (N8, N9 and N12). The highest solubility of NaDES containing LA may be attributed to LA's inherent solubilising effect (as demonstrated by solubility values on BNZ in LA90% and 80 %, which behaved as sample N15, **Fig. S2**), rather than solely relying on the formation of a supramolecular bonding network.

In the context of drug delivery, NaDES have mainly been studied for topical application. However, their high viscosity poses a challenge when considering their transformation into oral dosage forms. In a previous study (Albertini et al., 2023), we proposed capsule filling as a possible strategy for delivering drug-loaded NaDES to adults. Nevertheless, capsules may not be the most suitable option for young children.

Designing liquid or semisolid dosage forms could enhance swallowability compared to oral tablets or capsules, thereby improving acceptability among children. Our results demonstrated that diluting BNZ-NaDES systems with water significantly decreased drug solubility (Fig. 1**B,C**). Therefore, incorporating natural-derived polysaccharides such as xanthan gum (XG) into EGs with minimal water addition provides a feasible approach for administering drug-NaDES solutions. EGs with 5 mg/mL BNZ can be conveniently administered as oral soft gels packed in 5 mL stick-packs twice a day (with each unit providing a BNZ dose of 25 mg). This approach offers a practical and viable delivery option for the paediatric population.

Three NaDES (N8, N9 and N12) were transformed in EGs by adding 1 % w/w of XG and small amount of water (10 or 15 % w/w). The rheological study revealed a strong synergistic effect between XG and NaDES in determining the viscoelastic behaviour of the final gelled systems. The control sample, obtained by gelling water with the same XG amount, exhibited weak gel behaviour at 25 °C and behaved like a solution at physiological temperature, with a sol–gel transition between 37 and 25 °C (see Fig. 4**C,D,F**). In the XG gel, the presence of the polymeric chains implies a T_{2m} reduction from that of free water (≈ 4000 ms)(Coviello et al., 2013) to 1321 ms (see **Table S5**). Indeed, it is well known that in hydrogels, the polymeric network reduces the relaxation time (both T_{1m} and T_{2m}) of the embedded water molecules, and this reduction becomes more pronounced with a tight polymeric network. The shear modulus values (Table 4) and the magnetic relaxation properties (Fig. 4**A,B**) revealed the distinctive rheological-structural properties of EG@N, which differed from both the XG gels and from the starting NaDES. The latter are Newtonian viscous liquids at 37 °C (**Fig. S4**). Overall, the rheological and low field NMR data suggested a bimodal structure of EGs, as schematically represented in Scheme 2.

The two peaks of Fig. 4**D** correspond to two distinct regions within the EG@N structure:

i. a **water-rich region** consisting of a supramolecular hydrogen-bonded network involving NaDES, XG and a large amount of water (main peak in Fig. 4**D**). Polymer chains are connected to junctions (depicted as white small circles in Scheme 2) resulting in a labile structure characterised by weak interactions (smaller λ_1) and by transversal and longitudinal relaxation times T_{21} and T_{11}. This region occupies the largest volume (higher g_1) of the EG@N. Notably, the water relaxation times of EG@N fall between those of XG gel and original NaDES (very low water content). Accordingly, the reduction of T_{2m} and T_{1m} values in NaDES (N8, N9, N12 – see **Table S5**) are proportional to water content: the lower the water content, the shorter the relaxation time. The higher water content could be the reason for polymer junction lability.
ii. a **water-poor region** characterised by a denser and more rigid polymeric network. This region occupies the lower volume of EG@N (smaller peak of Fig. 4**D**) and exhibits more stable polymer junctions (grey circles in Scheme 2) as indicated by higher λ_i. The smaller relaxation times (T_{12} and T_{22}, **Table S5**) in this region can be attributed to the role of water: as the water content in the NaDES-XG network decreases, the crosslinks become stronger and more stable.

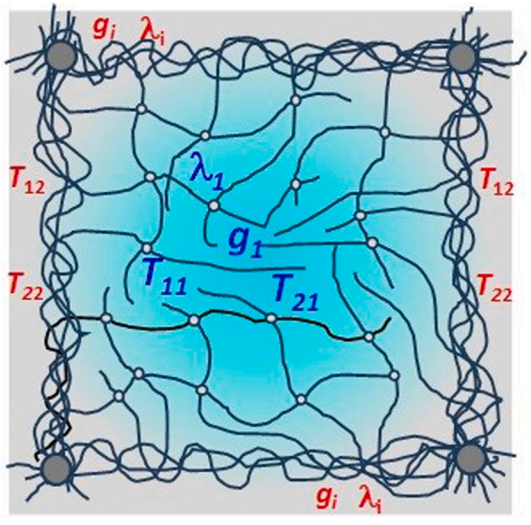

Scheme 2. Schematic representation of EGs structure. The light blue zone indicates the region characterised by a water-rich NaDES XG network characterised by transversal and longitudinal relaxation times T_{21} and T_{11}, respectively, and by the rheological parameters g_1 (elastic modulus) and λ_1 (mechanical relaxation time). The external grey zone indicates the water-poor rigid NaDES XG region characterised by transversal and longitudinal relaxation times T_{22} and T_{12}, respectively.

The crucial role of water in forming the hydrogel as well as EGs based on XG has been underlined. A recent study investigated semisolid EGs formed with up to 10 % XG and a small water amount (10 % w/w). The findings revealed that water was essential not only for preparing EGs based on ChCl but also for their physical stability (Zeng et al., 2020). Results indicated that gelation induced by XG resulted in the crystallization of NaDES components. This phenomenon was attributed to the removal of water molecules from NaDES by the XG polymer chains; consequently, supramolecular hydrogen bonding networks rearranged, leading to the reappearance of crystals. In the context of this study, BNZ-loaded EG@N maintained their structure unchanged over a period of 6 months, showing no phase modifications or drug crystallization (as indicated in **Table S1**). Furthermore, rheological data demonstrated that BNZ-loaded EG@N exhibit viscoelastic properties suitable for their intended application as oral soft gels, both at room temperature (25 °C) and after administration (37 °C).

In addition to suitable rheological properties, evaluating the biocompatibility, dissolution performance, and pharmacokinetic profiles is crucial to assess the feasibility of EG@N for BNZ delivery. The MTT assay conducted on gingival fibroblasts revealed a significant toxic effect specifically for EG@N15, regardless of the drug loading. This toxicity is likely associated with the high LA amount and the reduced extent of intramolecular H-bonds in the HPMC-based EGs compared to other EG@N formulations. In fact, EG@N formulations containing either citric or malic acid, despite having a similar pH value to N15 (as shown in Table 1), exhibited excellent cell viability after incubation. Similar positive results were obtained for betaine NaDES with malic acid and proline or glucose (1:1:1), indicating high cell tolerance (Radošević et al., 2018). In contrast, Popovic et al. observed cytotoxic profiles when combining ChCl in a 1:1 M ratio with various organic acids (citric, malic and lactic) on normal fibroblast MRC-5 cells (Popović et al., 2023). It is worth mentioning that in that study, the dilution of each combination of tested HBA: HBD with a substantial amount of water (20 wt%) could have partially disrupted the H-bonding network, leading to an increase presence of free–COOH moieties. For EG@N8, 9 and 12, the systems interact differently with cells as the water added during gelation was bound with XG.

BNZ release studies from EGs were then conducted trying to mimic the oral administration of gels to toddlers. Analysing Fig. 2**A**, it can be deduced that the release profiles in SGF are influenced by the viscosity of EGs: the more viscous fluid (EG@N12), the better controlled drug release. Despite the dilution of EGs into SGF, the supramolecular EGs maintained a supersaturated system. Upon further dilution in SIF, the EGs structure was disrupted, some level of supersaturation persisted, particularly in the case of EG@N8. This condition could potentially drive BNZ absorption. Subsequently, in vivo studies compared the performance of two selected EG@N formulations: EG@N8 and EG@N12. These formulations differ in viscosity (as shown in Fig. 4**A**) and composition.

In pharmacokinetic and bioavailability studies, BNZ was

administered to rats using doses of 1 mg/kg and 10 mg/kg for intravenous and oral routes, respectively. These doses ensured that plasmatic concentrations did not exceed 10 μg/mL, a value slightly lower than maximum plasmatic BNZ levels observed in previous rat studies (approximately 11 μg/mL) (Davanço et al., 2015). Futhermore, the recommended oral dose of 10 mg/kg per day aligns with paediatric treatment during the acute stage of the disease (Pérez-Molina and Molina, 2018) and it results 10 times lower than the BNZ dose causing oesophageal toxicity in rats (100 mg/kg) (de Castro et al., 2003). The BNZ profile in rat bloodstream after intravenous administration (Fig. 5**A**) exhibited concentration values similar to other known BNZ profiles, considering dose normalization (Morilla et al., 2004). The calculated half-life, corresponding to approximately two hours (based on the intravenous profile, Fig. 5**A**), aligns with existing BNZ half-life values in rodents (Davanço et al., 2015; Morilla et al., 2004; Perin Luísa et al., 2017). Moreover, since CD also involves the brain, we evaluated the BNZ's profile over time in the CNS of rats as well. The results (Fig. 5**B**) confirmed BNZ's ability to penetrate the brain of rodents from the bloodstream (Perin Luísa et al., 2017). The mean value of the BNZ concentration ratios (R) between CSF and bloodstream was about 0.5, indicating a marked ability of BNZ to penetrate the CNS. Notably, upon analysing the profile of raw BNZ in the bloodstream of rats following oral administration (Fig. 5**C**), an oral absolute bioavailability of approximately 4 % was obtained. This confirms the poor absorption capacity of this drug via the oral route. On the other hand, a mean value of the ratio R of about 0.5 (the same calculated after intravenous administration) was obtained from the profile of raw BNZ in the CSF of rats (Fig. 5**D**), supporting the ability of BNZ to permeate the CNS even after its oral administration. These findings indicate that the orally administered BNZ can exhibit therapeutic effects directly in the brain against CD, whose acute phase, usually occurring in children, causes death in approximately 10 % of patients due to encephalomyelitis (Prata, 2001).

The bloodstream BNZ concentration following the oral administration of the raw drug mixed with palatable food is comparable in magnitude to those obtained by the administration of BNZ formulated as a water suspension in the presence of Arabic gum, when doses are normalized (Morilla et al., 2004). On the other hand, when rats received the neat BNZ water suspension (without excipients), drug concentration values were significantly lower than those here detected (approximately 4 to 14 times lower, considering dose normalisation) (Barrera et al., 2020; Leonardi et al., 2013). BNZ-cyclodextrin complexes or chitosan microparticulate devices were demonstrated to substantially increase (up to 10 times) plasmatic drug concentrations after oral administration to rats (Barrera et al., 2020; Leonardi et al., 2013). However, these increased values appear lower than our results obtained after the oral administration of raw BNZ in the presence of palatable food, taking into account the dose normalisation (Barrera et al., 2020; Leonardi et al., 2013). Additionally, interpolyelectrolyte complexes have been proposed as another strategy to enhance BNZ oral bioavailability, demonstrating a 30 % increase in BNZ absorption in dogs (García et al., 2018).

Interestingly, the oral administration of the BNZ-loaded EGs to rats increased the drug bioavailability from 4.2 % (raw drug) to 8.5 % (EG@N12) or 11.1 % (EG@N8), emphasizing relative bioavailability values of 201 % or 263 %, respectively, with respect to the raw drug (Table 5). The correlation between these results and the *in vitro* release profiles is noteworthy, confirming the efficacy of supramolecular EGs in promoting drug absorption.

EGs facilitated comparable increases in BNZ levels in the CSF of rats (as indicated by the AUC values in Table 5). These findings highlight the capacity of these novel oral formulations to enhance the therapeutic efficacy of BNZ against CD, resulting in more than a twofold increase in concentration at both peripheral and central levels compared to the raw drug. These properties suggest that EGs could be a valuable approach for treating CD during its acute phase and may contribute to countering the eradication of Trypanosoma cruzi in the CNS.

5. Conclusions

We have demonstrated that eutectogels (EGs), derived from NaDES gelation by a biocompatible and biodegradable biopolymer (xanthan gum), represent a green and sustainable formulation strategy. This method proved to be feasible and effective in enhancing the solubility and absorption of BNZ, which exhibits variable bioavailability after oral administration, particularly in paediatric patients. Rheology and low field NMR characterisation showed that EGs exhibit a peculiar supramolecular structure that remained unchanged upon storage and temperature change. These polysaccharide-based materials are easy to use and prepare, a key point for a successful industrial scale-up. The enhancement of BNZ concentrations in the bloodstream and cerebrospinal fluid of rats suggests not only the superior bioavailability achieved by EGs but also the potential to extend the therapeutic efficacy of the drug to the chronic phase of the disease, particularly in its early stages. EG@N8 and EG@N12 can therefore be proposed for the paediatric CD treatment, owing to their advantageous properties (higher bioavailability and ease of administration) compared to traditional orally administered dosage forms.

Funding

This research did not receive any specific grant from funding agencies in the public, commercial, or not-for-profit sectors.

CRediT authorship contribution statement

Beatrice Albertini: Writing – review & editing, Writing – original draft, Visualization, Project administration, Conceptualization. **Serena Bertoni:** Writing – review & editing, Formal analysis, Data curation. **Giorgia Nucci:** Investigation. **Giada Botti:** Investigation. **Michela Abrami:** Investigation. **Stefano Sangiorgi:** Investigation. **Sarah Beggiato:** Investigation. **Cecilia Prata:** Investigation. **Luca Ferraro:** Writing – original draft, Resources, Methodology, Formal analysis. **Mario Grassi:** Writing – original draft, Resources, Methodology, Formal analysis. **Nadia Passerini:** Supervision, Resources. **Beatrice Perissutti:** Writing – review & editing, Writing – original draft, Visualization, Project administration, Conceptualization. **Alessandro Dalpiaz:** Writing – review & editing, Writing – original draft, Visualization, Validation, Resources.

Declaration of competing interest

The authors declare the following financial interests/personal relationships which may be considered as potential competing interests: [Giorgia Nucci reports financial support was provided by Fondazione Famiglia Parmiani, Bologna. If there are other authors, they declare that they have no known competing financial interests or personal relationships that could have appeared to influence the work reported in this paper.].

Data availability

Data will be made available on request.

Acknowledgments

We acknowledge "Fondazione Parmiani" (Bologna, Italy) for funding a one-year fellowship to Giorgia Nucci and Prof. Gabriella Teti of University of Bologna for kindly providing us the Human Gingival Fibroblasts (HGF) cell model.

Appendix A. Supplementary material

Supplementary data to this article can be found online at https://doi.

org/10.1016/j.ijpharm.2024.124417.

References

Abrami, M., Bignotti, F., Baldi, F., Spagnoli, G., Biasin, A., Grassi, L., Grassi, G., Grassi, M., 2023. Rheological and low field NMR characterization of hydrophobically-modified PEG hydrogels for drug delivery. Int. J. Pharm. 637, 122882 https://doi.org/10.1016/j.ijpharm.2023.122882.

Albertini, B., Bertoni, S., Sangiorgi, S., Nucci, G., Passerini, N., Mezzina, E., 2023. NaDES as a green technological approach for the solubility improvement of BCS class II APIs: an insight into the molecular interactions. Int. J. Pharm. 634, 122696 https://doi.org/10.1016/j.ijpharm.2023.122696.

Altcheh, J., Moscatelli, G., Caruso, M., Moroni, S., Bisio, M., Miranda, M.R., Monla, C., Vaina, M., Valdez, M., Moran, L., Ramirez, T., Patiño, O.L., Riarte, A., Gonzalez, N., Fernandes, J., Alves, F., Ribeiro, I., Garcia-Bournissen, F., 2023. Population pharmacokinetics of benznidazole in neonates, infants and children using a new pediatric formulation. PLoS Negl. Trop. Dis. 17, e0010850. https://doi.org/10.1371/journal.pntd.0010850.

Álvarez, M.S., Zhang, Y., 2019. Sketching neoteric solvents for boosting drugs bioavailability. J. Control. Release 311–312, 225–232. https://doi.org/10.1016/j.jconrel.2019.09.008.

Arrua, E.C., Hartwig, O., Loretz, B., Goicoechea, H., Murgia, X., Lehr, C.-M., Salomon, C. J., 2022. Improving the oral delivery of benznidazole nanoparticles by optimizing the formulation parameters through a design of experiment and optimization strategy. Colloids Surf. B Biointerfaces 217, 112678. https://doi.org/10.1016/j.colsurfb.2022.112678.

Arrúa, E.C., Seremeta, K.P., Bedogni, G.R., Okulik, N.B., Salomon, C.J., 2019. Nanocarriers for effective delivery of benznidazole and nifurtimox in the treatment of chagas disease: A review. Acta Trop. 198, 105080 https://doi.org/10.1016/j.actatropica.2019.105080.

Barrera, M.G., Tejada, G., Leonardi, D., Lamas, M.C., Salomón, C.J., 2020. A novel prototype device for microencapsulation of benznidazole in vitro/in vivo studies. AAPS PharmSciTech 21, 112. https://doi.org/10.1208/s12249-020-01659-3.

Bazzo, G.C., Pezzini, B.R., Stulzer, H.K., 2020. Eutectic mixtures as an approach to enhance solubility, dissolution rate and oral bioavailability of poorly water-soluble drugs. Int. J. Pharm. 588, 119741 https://doi.org/10.1016/j.ijpharm.2020.119741.

Bezerra, B.P., Pogoda, D., Perry, M.L., Vidal, L.M.T., Zaworotko, M.J., Ayala, A.P., 2020. Cocrystal polymorphs and solvates of the anti-trypanosoma cruzi drug benznidazole with improved dissolution performance. Cryst. Growth Des. 20, 4707–4718. https://doi.org/10.1021/acs.cgd.0c00490.

Bianchi, M.B., Zhang, C., Catlin, E., Sandri, G., Calderón, M., Larrañeta, E., Donnelly, R. F., Picchio, M.L., Paredes, A.J., 2022. Bioadhesive eutectogels supporting drug nanocrystals for long-acting delivery to mucosal tissues. Materials Today Bio 17, 100471. https://doi.org/10.1016/j.mtbio.2022.100471.

Botti, G., Bianchi, A., Pavan, B., Tedeschi, P., Albanese, V., Ferraro, L., Spizzo, F., Del Bianco, L., Dalpiaz, A., 2022. Effects of microencapsulated ferulic acid or its prodrug methyl ferulate on neuroinflammation induced by muramyl dipeptide. Int. J. Environ. Res. Public Health 19. https://doi.org/10.3390/ijerph191710609.

Campolmi, I., Angheben, A., Aliani, F.B., Spinicci, M., Bartoloni, A., Zammarchi, L., 2020. Chagas disease in Italy: updated estimates. Intern. Emerg. Med. 15, 1339–1343. https://doi.org/10.1007/s11739-020-02387-z.

Coviello, T., Matricardi, P., Alhaique, F., Farra, R., Tesei, G., Fiorentino, S.M., Asaro, F., Milcovich, G., Grassi, M., 2013. Guar gum/borax hydrogel: rheological, low field NMR and release characterizations. Express Polym Lett 7, 733–746.

Dai, Y., van Spronsen, J., Witkamp, G.-J., Verpoorte, R., Choi, Y.H., 2013. Natural deep eutectic solvents as new potential media for green technology. Anal. Chim. Acta 766, 61–68. https://doi.org/10.1016/j.aca.2012.12.019.

Dalpiaz, A., Gavini, E., Colombo, G., Russo, P., Bortolotti, F., Ferraro, L., Tanganelli, S., Scatturin, A., Menegatti, E., Giunchedi, P., 2008. Brain uptake of an anti-ischemic agent by nasal administration of microparticles. J. Pharm. Sci. 97, 4889–4903. https://doi.org/10.1002/jps.21335.

Dangre, P.V., Korekar, P.P., Borkar, M.R., Chaturvedi, K.K., Borikar, S.P., Pethe, A.M., 2023. Tailoring deep eutectic solvents to provoke solubility and bioavailability of naringin: implications of a computational approach. ACS Omega 8, 12820–12829. https://doi.org/10.1021/acsomega.2c08079.

Davanço, M.G., de Campos, M.L., Peccinini, R.G., 2015. Rapid and sensitive ultra-high-pressure liquid chromatography method for quantification of antichagasic benznidazole in plasma: application in a preclinical pharmacokinetic study. Biomed. Chromatogr. 29, 1008–1015. https://doi.org/10.1002/bmc.3386.

de Castro, C.R., Montalto de Mecca, M., Fanelli, S.L., de Ferreyra, E.C., Díaz, E.G., Castro, J.A., 2003. Benznidazole-induced ultrastructural and biochemical alterations in rat esophagus. Toxicology 191, 189–198. https://doi.org/10.1016/S0300-483X(03)00262-2.

de Moura Ferraz, L.R., Alves, A.É.G., da Silva Nascimento, D.D.S., e Amariz, I.A., Ferreira, A.S., Costa, S.P.M., Rolim, L.A., de Lima, Á.A.N., Neto, P.J.R., 2018. Technological innovation strategies for the specific treatment of Chagas disease based on Benznidazole. Acta Tropica 185, 127–132. https://doi.org/10.1016/j.actatropica.2018.02.008.

del Moral Sanchez, J.M., Gonzalez-Alvarez, I., Cerda-Revert, A., Gonzalez-Alvarez, M., Navarro-Ruiz, A., Amidon, G.L., Bermejo, M., 2018. Biopharmaceutical optimization in neglected diseases for paediatric patients by applying the provisional paediatric biopharmaceutical classification system. Br. J. Clin. Pharmacol. 84, 2231–2241. https://doi.org/10.1111/bcp.13650.

Echeverria, L.E., Morillo, C.A., 2019. American trypanosomiasis (Chagas Disease). Infect. Dis. Clin. North Am. 33, 119–134. https://doi.org/10.1016/j.idc.2018.10.015.

Faggian, M., Sut, S., Perissutti, B., Baldan, V., Grabnar, I., Dall'Acqua, S., 2016. Natural deep eutectic solvents (NADES) as a tool for bioavailability improvement: pharmacokinetics of rutin dissolved in proline/glycine after oral administration in rats: possible application in nutraceuticals. Molecules 21. https://doi.org/10.3390/molecules21111531.

Freerks, L., Sommerfeldt, J., Löper, P.C., Klein, S., 2020. Safe, swallowable and palatable paediatric mini-tablet formulations for a WHO model list of essential medicines for children compound – A promising starting point for future PUMA applications. Eur. J. Pharm. Biopharm. 156, 11–19. https://doi.org/10.1016/j.ejpb.2020.08.014.

García, M.C., Guzman, M.L., Himelfarb, M.A., Litterio, N.J., Olivera, M.E., Jimenez-Kairuz, A., 2018. Preclinical pharmacokinetics of benznidazole-loaded interpolyelectrolyte complex-based delivery systems. Eur J Pharm Sci 122, 281–291. https://doi.org/10.1016/j.ejps.2018.07.005.

García, M.C., Eberhardt, N., Sanmarco, L.M., Ponce, N.E., Jimenez-Kairuz, A.F., Aoki, M. P., 2021. Improved efficacy and safety of low doses of benznidazole-loaded multiparticulate delivery systems in experimental chagas disease therapy. Eur. J. Pharm. Sci. 164, 105912 https://doi.org/10.1016/j.ejps.2021.105912.

Gonzaga, B.M.S., Horita, S.I.M., Beghini, D.G., Gomes, F., Nisimura, L.M., dos Santos, I. B., Estato, V., de Araújo-Jorge, T.C., Garzoni, L.R., 2022. Effect of benznidazole on cerebral microcirculation during acute Trypanosoma cruzi infection in mice. Sci. Rep. 12, 21048. https://doi.org/10.1038/s41598-022-25056-x.

https://unitaid.org/news-blog/unitaid-commemorates-world-chagas-day-with-a-new-initiative-to-prevent-mother-to-child-transmission-of-the-disease/#en.

https://www.accessdata.fda.gov/drugsatfda_docs/label/2017/209570lbl.pdf.

Lapasin, R., Pricl, S., 1995. Rheology of Industrial Polysaccharides: Theory and Applications. London: Blackie. https://doi.org/10.1007/978-1-4615-2185-3.

Leonardi, D., Bombardiere, M.E., Salomon, C.J., 2013. Effects of benznidazole: cyclodextrin complexes on the drug bioavailability upon oral administration to rats. Int. J. Biol. Macromol. 62, 543–548. https://doi.org/10.1016/j.ijbiomac.2013.10.007.

Liu, Y., Friesen, J.B., McAlpine, J.B., Lankin, D.C., Chen, S.-N., Pauli, G.F., 2018. Natural deep eutectic solvents: properties, applications, and perspectives. J. Nat. Prod. 81, 679–690. https://doi.org/10.1021/acs.jnatprod.7b00945.

Luísa, P., da Silva, M., Rodrigo, F.K., da Silva, C., Mirelle, J., de Oliveira, M., Siqueira, F. A., Soares, R.L.E., Israel, M., Rodrigo, C.-O., Melo, V.P., de Abreu, C., Martins, C., 2017. Pharmacokinetics and tissue distribution of benznidazole after oral administration in mice. Antimicrob. Agents Chemother. 61 https://doi.org/10.1128/aac.02410-16.

Maximiano, F.P., Costa, G.H.Y., Souza, J., Cunha-Filho, M.S.S., 2010. Caracterização físico-química do fármaco antichagásico benznidazol. Quím. Nova 33, 1714–1719. https://doi.org/10.1590/S0100-40422010000800018.

Maximiano, F.P., de Paula, L.M., Figueiredo, V.P., de Andrade, I.M., Talvani, A., Sá-Barreto, L.C., Bahia, M.T., Cunha-Filho, M.S.S., 2011. Benznidazole microcrystal preparation by solvent change precipitation and in vivo evaluation in the treatment of Chagas disease. Eur. J. Pharm. Biopharm. 78, 377–384. https://doi.org/10.1016/j.ejpb.2011.03.003.

Mazzeti, A.L., Oliveira, L.T., Gonçalves, K.R., Schaun, G.C., Mosqueira, V.C.F., Bahia, M. T., 2020. Benznidazole self-emulsifying delivery system: a novel alternative dosage form for chagas disease treatment. Eur. J. Pharm. Sci. 145, 105234 https://doi.org/10.1016/j.ejps.2020.105234.

Mokhtarpour, M., Shekaari, H., Shayanfar, A., 2020. Design and characterization of ascorbic acid based therapeutic deep eutectic solvent as a new ion-gel for delivery of sunitinib malate. J. Drug Delivery Sci. Technol. 56, 101512 https://doi.org/10.1016/j.jddst.2020.101512.

Morilla, M.J., Montanari, J.A., Prieto, M.J., Lopez, M.O., Petray, P.B., Romero, E.L., 2004. Intravenous liposomal benznidazole as trypanocidal agent: increasing drug delivery to liver is not enough. Int. J. Pharm. 278, 311–318. https://doi.org/10.1016/j.ijpharm.2004.03.025.

Palmeiro-Roldán, R., Fonseca-Berzal, C., Gómez-Barrio, A., Arán, V.J., Escario, J.A., Torrado-Durán, S., Torrado-Santiago, S., 2014. Development of novel benznidazole formulations: Physicochemical characterization and in vivo evaluation on parasitemia reduction in Chagas disease. Int. J. Pharm. 472, 110–117. https://doi.org/10.1016/j.ijpharm.2014.06.015.

Pérez-Molina, J.A., Molina, I., 2018. Chagas disease. Lancet 391, 82–94. https://doi.org/10.1016/S0140-6736(17)31612-4.

Popović, B.M., Gligorijević, N., Aranđelović, S., Macedo, A.C., Jurić, T., Uka, D., Mocko-Blažek, K., Serra, A.T., 2023. Cytotoxicity profiling of choline chloride-based natural deep eutectic solvents. RSC Adv. 13, 3520–3527. https://doi.org/10.1039/D2RA07488E.

Prata, A., 2001. Clinical and epidemiological aspects of chagas disease. Lancet Infect. Dis. 1, 92–100. https://doi.org/10.1016/S1473-3099(01)00065-2.

Radošević, K., Čanak, I., Panić, M., Markov, K., Bubalo, M.C., Frece, J., Srček, V.G., Redovniković, I.R., 2018. Antimicrobial, cytotoxic and antioxidative evaluation of natural deep eutectic solvents. Environ. Sci. Pollut. Res. 25, 14188–14196. https://doi.org/10.1007/s11356-018-1669-z.

Saatkamp, R.H., Dos Santos, B.M., Sanches, M.P., Conte, J., Rauber, G.S., Caon, T., Parize, A.L., 2023. Drug-excipient compatibility studies in formulation development: a case study with benznidazole and monoglycerides. J. Pharm. Biomed. Anal. 235, 115634 https://doi.org/10.1016/j.jpba.2023.115634.

Santos Souza, H.F., Real, D., Leonardi, D., Rocha, S.C., Alonso, V., Serra, E., Silber, A.M., Salomon, C.J., 2017. Development and in vitro/in vivo evaluation of a novel benznidazole liquid dosage form using a quality-by-design approach. Trop. Med. Int. Health 22, 1514–1522. https://doi.org/10.1111/tmi.12980.

Scalise, M.L., Arrúa, E.C., Rial, M.S., Esteva, M.I., Salomon, C.J., Fichera, L.E., 2016. Promising efficacy of benznidazole nanoparticles in acute trypanosoma cruzi murine

model: in-vitro and in-vivo studies. Am. Soc. Trop. Med. Hyg. 95, 388–393. https://doi.org/10.4269/ajtmh.15-0889.

Simonazzi, A., Davies, C., Cid, A.G., Gonzo, E., Parada, L., Bermúdez, J.M., 2018. Preparation and Characterization of Poloxamer 407 Solid Dispersions as an Alternative Strategy to Improve Benznidazole Bioperformance. J. Pharm. Sci. 107, 2829–2836. https://doi.org/10.1016/j.xphs.2018.06.027.

Soares-Sobrinho, J.L., Santos, F.L.A., Lyra, M.A.M., Alves, L.D.S., Rolim, L.A., Lima, A.A. N., Nunes, L.C.C., Soares, M.F.R., Rolim-Neto, P.J., Torres-Labandeira, J.J., 2012. Benznidazole drug delivery by binary and multicomponent inclusion complexes using cyclodextrins and polymers. Carbohydr. Polym. 89, 323–330. https://doi.org/10.1016/j.carbpol.2012.02.042.

Song, Y.-Q., Venkataramanan, L., Hürlimann, M.D., Flaum, M., Frulla, P., Straley, C., 2002. T1–T2 correlation spectra obtained using a fast two-dimensional laplace inversion. J. Magn. Reson. 154, 261–268. https://doi.org/10.1006/jmre.2001.2474.

Streck, L., Sarmento, V.H.V., de Menezes, R.P.R.P.B., Fernandes-Pedrosa, M.F., Martins, A.M.C., da Silva-Júnior, A.A., 2019. Tailoring microstructural, drug release properties, and antichagasic efficacy of biocompatible oil-in-water benznidazol-loaded nanoemulsions. Int. J. Pharm. 555, 36–48. https://doi.org/10.1016/j.ijpharm.2018.11.041.

Sut, S., Faggian, M., Baldan, V., Poloniato, G., Castagliuolo, I., Grabnar, I., Perissutti, B., Brun, P., Maggi, F., Voinovich, D., Peron, G., Dall'Acqua, S., 2017. Natural deep eutectic solvents (NADES) to enhance berberine absorption: an in vivo pharmacokinetic study. Molecules 22. https://doi.org/10.3390/molecules22111921.

Teti, G., Orsini, G., Salvatore, V., Focaroli, S., Mazzotti, M.C., Ruggeri, A., Mattioli-Belmonte, M., Falconi, M., 2015. HEMA but not TEGDMA induces autophagy in human gingival fibroblasts. Front. Physiol. 6.

Urbina, J.A., 2010. Specific chemotherapy of chagas disease: relevance, current limitations and new approaches. Acta Trop. 115, 55–68. https://doi.org/10.1016/j.actatropica.2009.10.023.

Urbina, J.A., Docampo, R., 2003. Specific chemotherapy of chagas disease: controversies and advances. Trends Parasitol. 19, 495–501. https://doi.org/10.1016/j.pt.2003.09.001.

van den Berg, M.P., Romeijn, S.G., Verhoef, J.C., Merkus, F.W.H.M., 2002. Serial cerebrospinal fluid sampling in a rat model to study drug uptake from the nasal cavity. J. Neurosci. Methods 116, 99–107. https://doi.org/10.1016/S0165-0270(02)00033-X.

WHO Model List of Essential Medicines for Children - 8th list, 2021 https://www.who.int/publications/i/item/WHO-MHP-HPS-EML-2021.03.

Xia, H., Ren, M., Zou, Y., Qin, S., Zeng, C., 2020. Novel biocompatible polysaccharide-based eutectogels with tunable rheological, thermal, and mechanical properties: the role of water. Molecules 25. https://doi.org/10.3390/molecules25153314.

Zainal-Abidin, M.H., Hayyan, M., Ngoh, G.C., Wong, W.F., Looi, C.Y., 2019. Emerging frontiers of deep eutectic solvents in drug discovery and drug delivery systems. J. Control. Release 316, 168–195. https://doi.org/10.1016/j.jconrel.2019.09.019.

Zeng, C., Zhao, H., Wan, Z., Xiao, Q., Xia, H., Guo, S., 2020. Highly biodegradable, thermostable eutectogels prepared by gelation of natural deep eutectic solvents using xanthan gum: preparation and characterization. RSC Adv. 10, 28376–28382. https://doi.org/10.1039/D0RA03390A.